INSTITUTE OF PHYSICS PUBLISHING JOURNAL OF OPTICS B: QUANTUM AND SEMICLASSICAL OPTICS

J. Opt. B: Quantum Semiclass. Opt. **6** (2004) 97–105 PII: S1464-4266(04)65975-1

Synchronization scenario of two distant mutually coupled semiconductor lasers

Josep Mulet[1,2], **Claudio Mirasso**[1,3], **Tilmann Heil**[4] and **Ingo Fischer**[4,5]

[1] Departament de Física, Universitat de les Illes Balears, E-07122 Palma de Mallorca, Spain
[2] Research Centre COM, Technical University of Denmark, DTU-Building 345V, DK-2800 Lyngby, Denmark
[3] Electrical Engineering Department, 56-147C Engineering IV UCLA, Los Angeles, CA 90095-1594, USA
[4] Institute of Applied Physics, Darmstadt University of Technology, Schloßgartenstraße 7, D-64289 Darmstadt, Germany

E-mail: mulet@imedea.uib.es

Received 3 July 2003, accepted for publication 12 November 2003
Published 21 November 2003
Online at stacks.iop.org/JOptB/6/97 (DOI: 10.1088/1464-4266/6/1/016)

Abstract
We present numerical and experimental investigations of the synchronization of the coupling-induced instabilities in two distant mutually coupled semiconductor lasers. In our experiments, two similar Fabry–Perot lasers are coupled via their coherent optical fields. Our theoretical framework is based on a rate equation model obtained under weak coupling conditions. In both experiments and simulations, we find (achronal) synchronization of subnanosecond intensity fluctuations in concurrence with asymmetric physical roles between the lasers, even under symmetric operating conditions. We explore the synchronization of these instabilities with respect to the coupling strength and the injection current. We demonstrate the existence of a critical coupling strength, below which synchronization is lost; however, dynamical instabilities persist. Our model correctly reproduces the observed dynamical features over the entire investigated parameter space. We provide an intuitive explanation of the appearance of the achronal solution by analysing the dynamics of the injection phases of the optical fields.

Keywords: semiconductor lasers, injection locking, synchronization, nonlinear dynamics

1. Introduction

Coupled nonlinear oscillators have been extensively studied in the past due to the rich variety of possible behaviours and applications. Periodic and chaotic oscillations have been reported in a wide class of systems: chemical reactions, population dynamics, physiological interactions, coupled neurons, mechanical oscillators, lasers [1–4] etc. Investigations using semiconductor lasers (SCL) have several advantages. Firstly, the nonlinear dynamical behaviour of these lasers is widely understood. Secondly, the parameters of SCL are well known and some of them can be controlled accurately. Thirdly, SCL are the key devices for current telecommunication technologies. In a new development, interest in coupling and synchronization phenomena in SCL has been boosted by the proposal of novel communications systems using chaotic carriers [5–7].

Mutually coupled oscillators are of special interest since fundamental concepts, such as synchronization, were first discovered in these systems. In many real world systems, the coupled oscillators are spatially separated. As a consequence, the coupling exhibits a certain delay due to the propagation of the signal between the oscillators. Nevertheless, it is in many cases justified to neglect this delay because it is much shorter

[5] Author to whom any correspondence should be addressed.

than the internal timescales of the subsystems. However, if this condition is not fulfilled, delay can yield unexpected dynamical behaviours, mainly due to the additional degrees of freedom introduced into the system.

Most of the studies with coupled semiconductor lasers considered unidirectional injection from a master laser to a slave laser in order to achieve injection locking [8, 9] or synchronization of chaotic oscillations [5]. The first studies of weak mutually coupled semiconductor lasers with delay [10, 11] found an interesting type of synchronization, characterized by *localized* oscillations in one of the lasers. Under these conditions, the laser intensities generally undergo periodic or quasi-periodic oscillations. Recently, considering weak to moderate coupling conditions and long delay times, a new fascinating dynamical behaviour was found [12, 13]: the coupled lasers exhibit subnanosecond synchronized chaotic dynamics. Even in the case of identical devices, the roles between the lasers were found to be asymmetric, and a time lag between their dynamics was observed [12]. Since these discoveries, interest in the fundamental investigation of mutually delay coupled lasers has emerged. In [14, 15] the authors discussed the question of whether a rate equation model or the optical travelling wave model can correctly describe the coupled lasers. The authors found that both descriptions lead to similar behaviours when the coupling is kept to moderate values. Using the rate equation description it has been possible to obtain analytical expressions of the phase-locked monochromatic solutions (bidirectional injection locking) [14], stability of fixed points and periodic orbits [16], and semi-analytical predictions of the stability of synchronized chaotic solutions [17]. In spite of these advances, many aspects of the complex nonlinear dynamics, such as the mechanisms leading to synchronization with a time shift, are not yet fully understood.

In the first part of this paper, we present a detailed numerical and experimental investigation of the synchronization scenario of two delayed coupled SCL. This framework enables a joint description of the different dynamical behaviours of the system with their synchronization properties. We centre the discussion on the dynamical instabilities resulting from symmetric coupling of the lasers. Synchronization occurs upon increase of the coupling strength beyond a well defined threshold. Synchronization is robust in the sense that it appears for a wide range of currents and coupling strengths. Despite the large degree of symmetry in the system, we demonstrate that the system spontaneously selects a state of achronal synchronization characterized by a time lag between the dynamics of the lasers, and a large degree of correlation. The dynamical properties of the achronal solution are analysed using crosscorrelation techniques. The second part of the paper is devoted to providing an intuitive picture of the observed dynamics. We start analysing the stability of the chaotic isochronal solution. We find that the isochronal solution is unstable for any small fluctuation, e.g. due to spontaneous emission. Associated with the instability of the isochronal solution, we find the nontrivial dynamics of the optical injection phases of the lasers. The leader–laggard role of the lasers turns out to be related to the evolution of the optical phases. Moreover, a simplified model describing the phase dynamics corroborates the fact that the isochronal solution is intrinsically unstable against fluctuations.

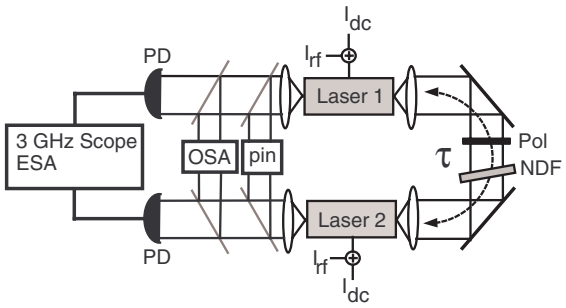

Figure 1. Scheme of the experimental setup of two mutually coupled SCL with polarizer (Pol), neutral density filter (NDF), optical spectrum analyser (OSA) and electrical spectrum analyser (ESA).

2. Experimental setup

Figure 1 depicts a schematic of the experimental setup. Two device-identical SCL are mutually coupled with a delay via their coherent optical fields. The distance between the lasers determines the coupling delay by the propagation of the light between the lasers. In experiments, the one-way coupling delay amounts to $\tau = 4$–5 ns. The lasers are two uncoated Hitachi HLP1400 Fabry–Perot SCL produced from the same wafer in order to achieve the highest possible degree of symmetry in the system. The temperature of each laser is stabilized to better than 0.01 K, and selected such that the free-running frequencies of the two lasers match with an accuracy better than 1 GHz. The polarizer guarantees a coherent coupling between the lasers via the dominant transverse electric (TE) mode of the optical field. A neutral density filter placed between the two SCL controls the coupling strength. In the present experiment, a maximum amount of 5% of the output power of each laser is injected into its counterpart. In the detection branch of the setup, two photoreceivers with a bandwidth of 6 GHz are used to detect the intensity dynamics of both lasers simultaneously via their rear facet emission. The signal of the photoreceivers is analysed by a fast digital oscilloscope of 3 GHz analogue bandwidth recording the temporal waveforms, and an electrical spectrum analyser recording the corresponding rf-spectra. In addition, the optical spectra of the lasers are monitored with a grating spectrometer with a resolution of 0.1 nm. Finally, the time averaged output power of both lasers is detected by two p–i–n photodiodes.

3. The model

In a general case, the optical propagation in three coupled cavities determines the coupling between the lasers of figure 1. The coupling terms have quite involved expressions [18]. However, the problem can be reduced to a bidirectional injection problem with time delay in the limit of weak coupling conditions [14]. Each laser can be then described by means of rate equations for the electric field and the total carrier density. In contrast to previous studies of coupled solid-state lasers [19], the carrier rate equations are independent since the lasers are spatially separated. The weak coupling limit is justified since the concept of synchronization is intrinsically linked to weakly

Table 1. Symbols, meanings and numerical values. The dimensionless gain constant is $a \equiv gN_t/\gamma$ and the threshold current is $I_{th}^{sol} = I_t(1 + 1/a) \approx 60$ mA.

Symbol	Meaning	Value	Dimensions
α	Linewidth enhancement factor	4.0	—
γ	Cavity loss rate	243	ns^{-1}
g	Differential gain	3.2×10^{-6}	ns^{-1}
κ	Coupling rate	$\sim$20	ns^{-1}
τ	Coupling time	4–5	ns
γ_e	Carrier decay rate	1.66	ns^{-1}
N_t	Carrier number at transparency	1.5×10^8	—
ε	Gain suppression	10^{-1}	—
β_{sp}	Spontaneous emission factor	10^{-5}	—

interacting subsystems [20]. Otherwise the system of figure 1 should be considered as a single compound-cavity laser. In a practical situation, the amount of injected light from one laser to its counterpart is controlled by varying the transmittivity of an optical coupler located within the interlaser spacing (the neutral density filter in figure 1).

The dynamics of the slowly-varying amplitude of the electric fields $A_{1,2}(t)$ and the respective carrier inversions $D_{1,2}(t)$ (scaled to the transparency density) is governed by

$$d_t A_{1,2}(t) = \tfrac{1}{2}(1 - i\alpha)\gamma[\mathcal{G}_{1,2}(t) - 1]A_{1,2}(t) + \kappa_c e^{i\Omega_0\tau} A_{2,1}(t - \tau) + F_{A_{1,2}}(t), \quad (1)$$

$$d_t D_{1,2}(t) = \gamma_e[\mu - D_{1,2} - \mathcal{G}_{1,2}|A_{1,2}|^2], \quad (2)$$

$$\mathcal{G}_{1,2}(t) = \frac{a D_{1,2}}{1 + \varepsilon|A_{1,2}|^2}, \quad (3)$$

with κ_c being the coupling rate, τ the one-way coupling time and the suffices 1, 2 being used to label the lasers. Analysing equation (1) we find an interpretation of the terms $\kappa_c A_{2,1}(t-\tau)$: they describe the mutual delayed injection from one laser to its counterpart. The injection current normalized to the transparency value $I_t \equiv e\gamma_e N_t$ is given by $\mu \equiv I/I_t - 1$. The current is also commonly referred to the solitary threshold current by means of $p = I/I_{th}^{sol}$. Finally, we have included Langevin noise terms to the field equations in order to account for spontaneous emission processes. These terms have zero mean, $\langle F_{A_{1,2}}(t)\rangle = 0$, and correlation $\langle F_{A_i}(t)F^*_{A_j}(t')\rangle = 2\beta_{sp}\gamma\delta_{i,j}(D_i + 1)\,\delta(t - t')$, with β_{sp} the spontaneous emission factor. In simulations, we consider identical parameters in both SCL. Hence, the equations are perfectly symmetric under the interchange of the lasers, except for noise terms. The meaning and numerical values of the parameters, taken from the actual experimental conditions, are given in table 1.

The optical coupling is coherent in the sense that it depends on the amplitude and, more importantly, the optical phase of the electric fields. This fact becomes evident when expressing equation (1) as equations for the optical intensity and phase, through $A_{1,2}(t) = \sqrt{P_{1,2}(t)}e^{i\varphi_{1,2}(t)}$, which finally leads to

$$d_t P_{1,2}(t) = \gamma[\mathcal{G}_{1,2}(t) - 1]P_{1,2}(t) + 2\kappa_c\sqrt{P_{1,2}(t)P_{2,1}(t - \tau)}\cos(\eta_{1,2}(t) + \varphi_0) + 4\beta_{sp}\gamma(D_{1,2} + 1) + F_{P_{1,2}}(t), \quad (4)$$

$$d_t\varphi_{1,2}(t) = -\frac{\alpha}{2}\gamma[\mathcal{G}_{1,2}(t) - 1] + \kappa_c\sqrt{\frac{P_{2,1}(t - \tau)}{P_{1,2}(t)}}\sin(\eta_{1,2}(t) + \varphi_0) + F_{\varphi_{1,2}}(t), \quad (5)$$

where $\eta_{1,2}(t) \equiv \varphi_{2,1}(t - \tau) - \varphi_{1,2}(t)$ stand for the injection phases from laser 1 to laser 2 and vice versa, whereas $\varphi_0 \equiv \Omega_0\tau \bmod 2\pi$ is the optical phase accumulated in one-way propagation. $F_{P_{1,2}}(t)$ and $F_{\varphi_{1,2}}(t)$ represent four independent real Langevin noise sources. A generic monochromatic solution can be expressed as $\varphi_1(t) = -\Omega t$ and $\varphi_2(t) = -\Omega t + \phi$, so the injection phases lock to $\eta_1(t) = \Omega\tau + \phi$ and $\eta_2(t) = \Omega\tau - \phi$, respectively. The equations are invariant under addition of multiples of 2π to $\eta_{1,2}(t)$, as a result of the invariance under time translations. The relative phase shift between lasers can be described by $\Delta\eta(t) \equiv \eta_1(t) - \eta_2(t) = 2\phi$. The relevance of the injection phases shall be addressed in section 6.

It is worth recalling that several hypotheses are implicit in the derivation of these equations: single-longitudinal mode operation and a common emission frequency Ω_0 of the free-running lasers, and weak coupling. The equations are only valid to lower order in ξ (coupler transmittivity) and neither passive feedback reflections involving terms like $A_{1,2}(t - 2\tau)$ nor higher-order corrections, for example, are accounted for at this order of approximation. We notice that although the higher-order terms are always present, their relative influence diminishes when the coupler transmittivity approaches zero. Although the coupled lasers exhibit multimode-emission in the experiments we will show that the single-mode approximation is sufficient to explain the synchronization scenario.

4. Synchronization scenario

We centre our discussion on the instabilities that arise under weak to moderate coupling conditions (a maximum of 5% of the light emitted is injected) and long coupling delay times. We explore the behaviour of the system under variations of two easily accessible parameters, namely, the coupling rate κ_c and the current injection that we consider to be the same in both lasers.

Operating close to the solitary threshold and when the coupling rate exceeds a certain value κ_c^I, the two laser intensities display a behaviour that consists of irregular pulsations with little correlation between them. This point defines the onset of the coupling-induced instabilities. Increasing the coupling strength further, the instabilities reshape into similar pulsations but now accompanied by sudden power dropouts followed by a gradual recovery of the optical power. The interesting fact is that the pulsations in both lasers start to display a good correlation only beyond a second threshold for the coupling rate κ_c^{II}.

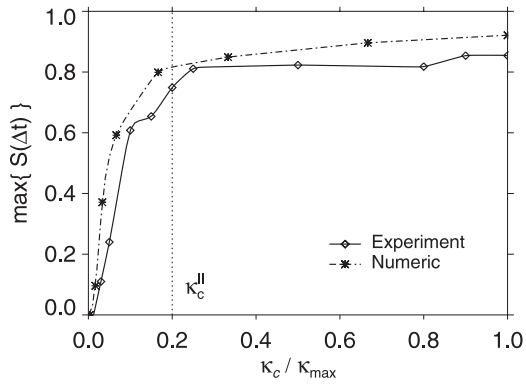

Figure 2. Numerical and experimental comparison of the maximum degree of correlation achieved as function of the coupling strength. Parameters from table 1 except $\tau = 4$ ns and $p = 1$.

In order to better characterize this twofold threshold behaviour, we introduce the crosscorrelation function [21, 22] $S(\Delta t)$ between two variables $x_1(t)$ and $x_2(t)$ (with mean values being subtracted) as

$$S(\Delta t) = \frac{\langle x_1(t)x_2(t+\Delta t)\rangle}{\sqrt{\langle x_1^2(t)\rangle\langle x_2^2(t)\rangle}}, \tag{6}$$

where $\langle\cdot\rangle$ means time average. We look for the time shift Δt where the maximum correlation of the laser intensities, $\max\{S(\Delta t)\}$, referred to as correlation degree, is achieved. In figure 2, we observe that, as the coupling strength is increased, the correlation degree increases very rapidly from zero until it reaches a saturation value. Above this critical value, the correlation degree does not significantly increase, displaying a plateau with a relatively high value, ∼0.9. The maximum coupling rate accessible in the experiment roughly corresponds to $\kappa_{\max} \approx 25\ \text{ns}^{-1}$. It is worth noting the excellent agreement between theoretical and experimental dependences, demonstrating that a large degree of synchronization is possible for a wide range of coupling strengths. High correlation degree (0.8–0.9) persists for injection currents typically below twice the solitary threshold current. These results indicate that large degree of synchronization is achieved when both lasers operate in the equivalent regime IV of a laser with optical feedback [23]. The correlation degrades when the injection is increased beyond this value, where the optical spectra display a broad band of frequencies (∼20 GHz wide) indicating that they are operating within a fully-developed coherence collapse regime [24].

The large correlation between the intensities motivates us to further investigate the transition towards synchronization of the coupling-induced instabilities. A typical example of the dynamics beyond the second coupling threshold ($\kappa_c > \kappa_c^{II}$) is depicted in figure 3. In numerical simulations we took a coupling rate of $\kappa_c = 20\ \text{ns}^{-1}$, in line with experimental conditions. We represent the intensity traces of laser one in black and laser two in grey lines. When they operate close to the solitary threshold current, as depicted in figure 3(a), we find that the low frequency dynamics consists in power dropouts that display a good correlation between the two lasers. Power dropouts appear in a wide range of coupling rates and injection currents close to the solitary laser threshold.

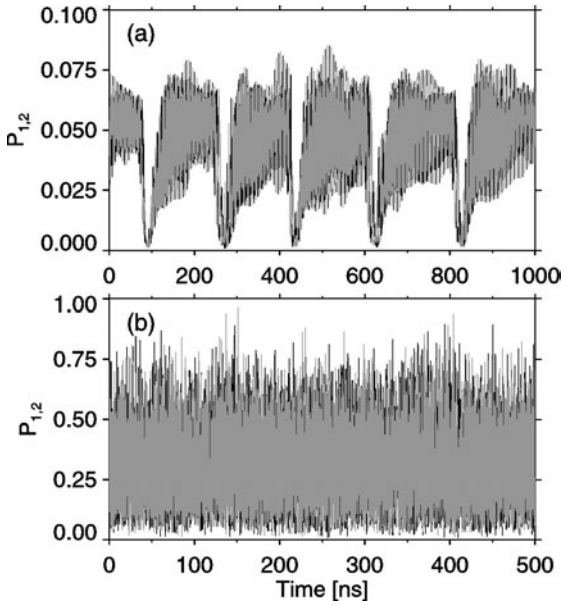

Figure 3. Numerical time traces of the laser intensities for injection current (a) $p = 0.98$ and (b) $p = 1.17$. The coupling rate is $\kappa_c = 20\ \text{ns}^{-1}$ and $\tau = 4$ ns.

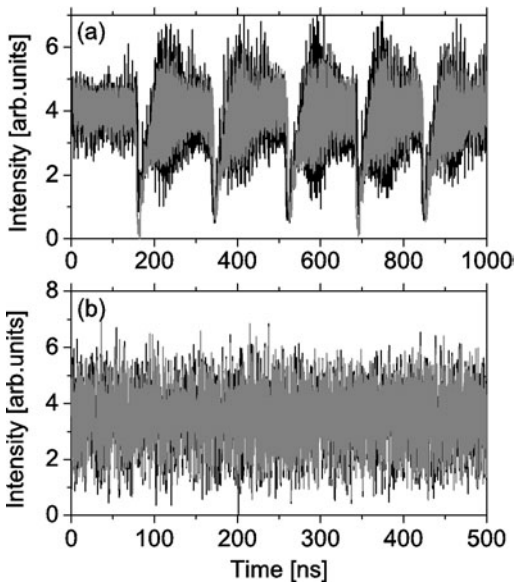

Figure 4. Experimental time traces of the intensity emitted by the two lasers when running under same conditions as figure 3.

For higher injection currents, power dropouts disappear and the system enters a coherence collapsed (CC) regime (see figure 3(b)). These numerical results are in good agreement with experimental traces shown in figure 4. The mean time between dropouts, the dependence on the injection current and the transition to the CC regime are also well reproduced by the rate equation model.

5. Achronal synchronization

5.1. Characterization

Zooming up into nanosecond timescales, we observe that the optical intensities are organized in a sequence of fast irregular

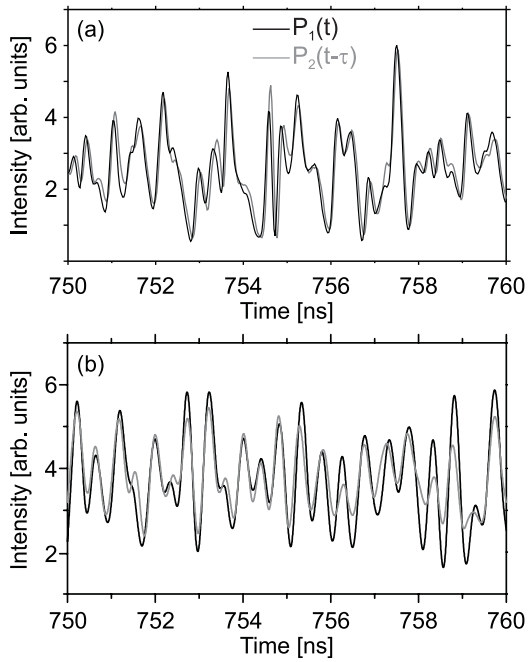

Figure 5. Subnanosecond synchronized dynamics between two consecutive power dropouts for (a) numerical and (b) experimental results. The time shift between the lasers has been compensated for. The same conditions as figure 3 apply except $p = 1$. The numerical traces have been filtered at 3 GHz bandwidth corresponding to the analogue bandwidth of the experimental detection setup.

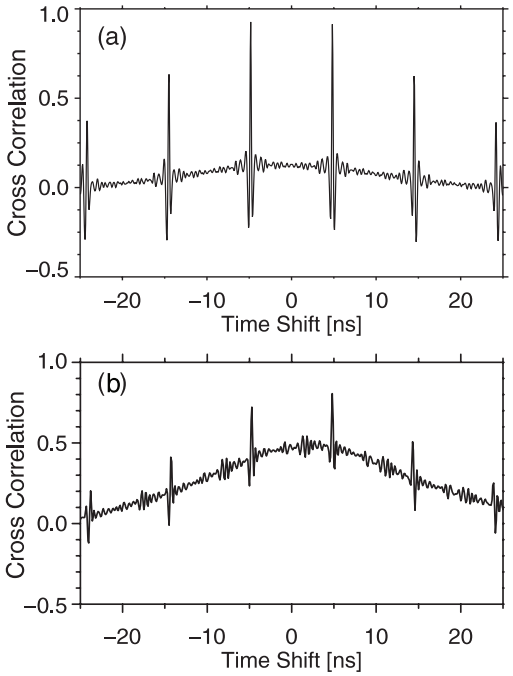

Figure 6. (a) Numerical and (b) experimental crosscorrelation function. Parameters: $\tau = 4.8$ ns, $\kappa_c = 20$ ns^{-1} and $p = 1$.

pulses, as depicted in figure 5. This fast pulsating behaviour appears to be well correlated only if one series is shifted with respect to the other by a time, τ, that precisely corresponds to the coupling time. The solution where the dynamics of the lasers occurs with such a time shift is referred to as leader–laggard operation [12] or achronal synchronization [17]. The dynamical properties of the achronal state are particularly interesting because they originate from the bidirectional coupling of perfectly symmetric subsystems. It is worth noting that the achronal state is not a perfectly synchronized solution of our system; it would only be possible for a periodic oscillation. Consequently, the maximum correlation degree attainable is a consequence of a fundamental limitation of the system. Next, we characterize this solution using two standard techniques, namely, crosscorrelation functions and generalized return plots.

A standard tool for detecting the dependences between the two laser intensities is the crosscorrelation function $S(\Delta t)$ defined in equation (6). The crosscorrelation function obtained from numerical traces, figure 6(a), displays dominant peaks at odd resonances of the coupling time, that is to say, $\Delta t = \pm n\tau$ with $n = 1, 3, 5, \ldots$. Consequently, successive peaks are separated by a distance 2τ that corresponds to a roundtrip in the interlaser space. The correlation at the successive peaks decays when the index n increases while it is almost vanishing near the zero shift $\Delta t = 0$, indicating that fluctuations occurring at the same time are independent. The experimental correlation function, obtained from the time traces in figure 4, is shown in figure 6(b). The function displays the same features as described above: the peaks are located at the correct positions with similar values of correlation degree as those obtained numerically. These results are found for a wide range of injection currents close to threshold.

The quality of the synchronization can be also studied by plotting the intensity of laser 2 versus the intensity of laser 1. We note that we need to time shift one signal, otherwise only a cloud of points is obtained. In order to decide which is the most suitable direction for the time shift of the series we calculate the crosscorrelation function. The latter exhibits two maxima located at $\Delta t = -\tau$ and τ. These two maxima have the same amplitude if we take long enough time series. This fact indicates that we can arbitrarily shift one series with respect to the other by a time $-\tau$ or $+\tau$ and get the same correlation degree, although we stress that the series are not periodic. If we take a short time series, e.g. including a few dropouts, the crosscorrelation function is asymmetric, determining a suitable direction for the shift. When a signal is moved in this direction, a squeezed cloud of points arranged around a 45° straight line is obtained. As can be seen in figure 7, experimental and numerical characteristics are in agreement. The dispersion of the points with respect to the linear tendency is linked to the maximum correlation degree achieved. We recall that the maximum degree of correlation increases from zero very rapidly when the coupling strength is increased until it reaches a saturation value, as discussed for figure 2.

5.2. Instability of the isochronal solution

We have performed deterministic numerical simulations to decide whether the achronal state appears as a general property of the system or is just a consequence of the noise sources always present in the experiment and explicitly included in the equations. In figure 8, we artificially switch off the noise and we prepare both lasers to start from identical initial conditions. We find that the system evolves in an isochronal

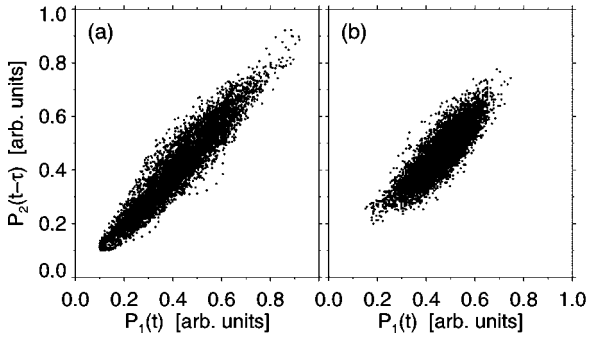

Figure 7. (a) Numerical and (b) experimental generalized return plots for the same conditions as figure 6. The maximum correlation degree is ∼0.85 in both cases.

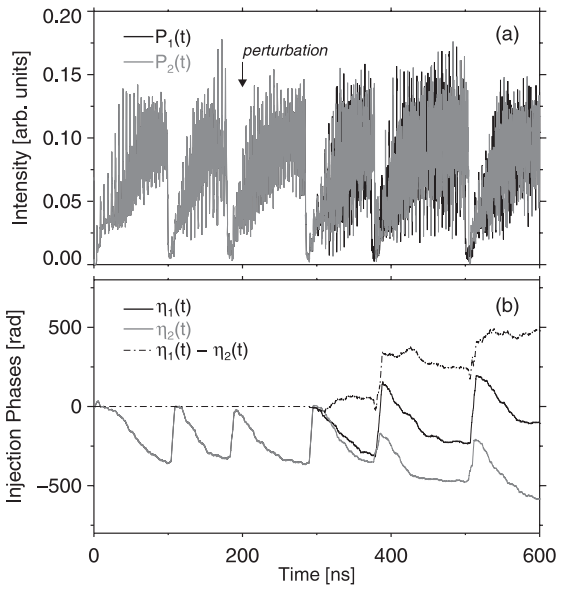

Figure 8. Deterministic numerical simulation describing the destabilization of the isochronal solution due to an external perturbation applied at $t = 200$ ns. (a) Intensity time traces filtered at 3 GHz and (b) the dynamics of the injection phases. Parameters: $\tau = 5$ ns, $\kappa_c = 20\ \mathrm{ns}^{-1}$ and $p = 1$.

state ($P_1(t) = P_2(t)$, $D_1(t) = D_2(t)$) until a small perturbation is externally introduced at $t = 200$ ns (the intensity of laser 1 is modified by 1%). In spite of the absence of noise for $t > 200$ ns, this small perturbation is able to destabilize the isochronal solution, and the system evolves towards the achronal state. Since the system remains in the achronal state for any arbitrarily long integration times, we give evidence that the isochronal solution is unstable in our system, and that the spontaneous emission prevents the observation of such a state. The rest of the paper is devoted to providing an intuitive explanation of (i) the instability of the isochronal solution and (ii) the properties of the achronal state.

Previous studies [16, 17] suggested that the mechanisms leading to the instability of the isochronal solution are related to the role of the optical phases. In order to clarify this point, we track the injection phases, $\eta_{1,2}(t)$, defined previously in section 3. During the initial transient and before the perturbation is applied, the two injection phases evolve in an identical fashion, $\eta_1(t) = \eta_2(t)$, as can be seen in figure 8(b). The injection phases move close to the fixed points of the

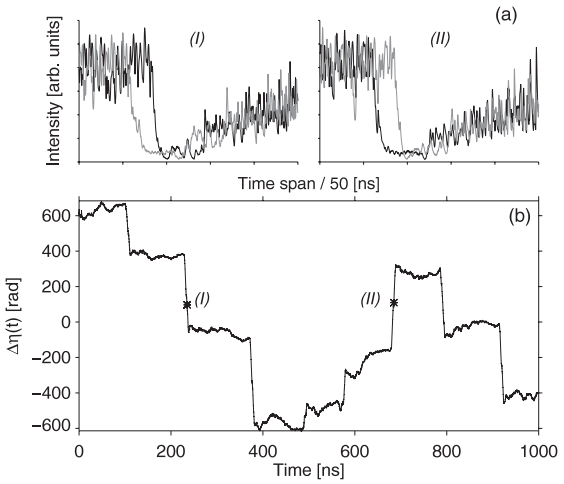

Figure 9. (a) Detail of two different power dropouts and respective recovery transients and (b) the dynamics of the relative injection phases. Parameters: $\tau = 5$ ns, $\kappa_c = 20\ \mathrm{ns}^{-1}$ and $p = 1$.

compound system [14], displaying a chaotic itinerancy towards low frequencies very similar to what happens in SCL with optical feedback [25]. Power dropouts produce a rapid increase of the injection phases, consequently shifting the emission to higher frequencies. When the perturbation is applied, this operating mode turns out to be unstable and the two injection phases separate. This fact confirms the existence of a phase instability that we shall discuss in section 6.

5.3. Change of role

In this section, we analyse the relationship between the leader–laggard roles of the lasers and the phase dynamics. We shall concentrate the discussion on the achronal solution that occurs for currents close to the solitary threshold. After a careful analysis of figures 3 and 4, we observe that power dropouts do not occur simultaneously in both lasers but with a time lag τ_0. In figure 9(a), we show two arbitrary dropouts taken from a long time series. In event (I) laser two drops first, whereas in case (II) laser one drops first. Interestingly, the difference between the injection phases, $\Delta\eta(t)$, has the intrinsic dynamics shown in figure 9(b). Large variations in $\Delta\eta(t)$ occur at the power dropouts, whereas $\Delta\eta(t)$ is approximately steady during the two consecutive dropouts. The difference in injection phases suddenly increases (decreases) when laser one (laser two) drops first. This behaviour can be understood if we realize that the effective coupling between the lasers is asymmetric during dropouts. In example (I), only laser 2, which drops first, continues receiving light from laser 1 during the period τ_0. The lack of feedback light after this time initiates the drop of laser 1. The scenario in example (II) is equivalent to (I), simply changing the labels of the lasers. During the recovery process, both laser intensities gradually increase making the coupling again symmetric so the lasers may compete for the leading role. The change in role of the lasers is also found in the experiments, as shown in figure 4(a).

In order to better understand the change in order of the power dropouts, we perform a statistical analysis [26]. Comparison with experiments is not available here because we did not take sufficiently long time series to allow for a

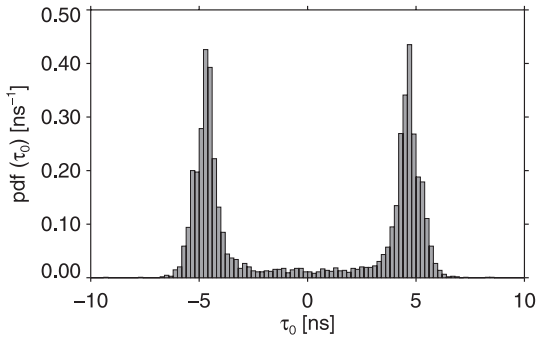

Figure 10. Probability density function of the time shift between power dropouts of the two lasers, τ_0, for $\tau = 5$ ns, $\kappa_c = 20\ \mathrm{ns}^{-1}$ and $p = 1.01$.

significant statistical analysis of dropout events. We define a time lag by means $\tau_0 \equiv \tau_1^k - \tau_2^k$, where τ_j^k stands for the kth dropout time of laser j. To decide whether a power dropout occurs or not, we look at those events where the laser intensity crosses below a predefined threshold. Hence, positive (negative) τ_0 means that laser 1 drops before laser 2. The probability distribution function of τ_0, shown in figure 10, is obtained from a large number of power dropouts ($\gtrsim 10^4$ events). We find that most of the dropouts occur at times $\tau_0 \approx \pm\tau$, whereas larger times are unlikely. The probability of synchronized dropouts, i.e. $\tau_0 \approx 0$, is rare although non-vanishing. The probability distribution function is symmetric around $\tau_0 = 0$, indicating that the number of events where laser 1 drops first is, on average, equal to the number where laser 2 drops first. This fact indicates that the statistical quantities, computed over long time intervals of an achronal state, are invariant under the interchange of the lasers, although at any time the leader and laggard roles are clearly defined.

5.4. Influence of noise

Spontaneous emission noise can have an influence on the dynamics, in particular during the power dropouts where the laser intensities reach low levels. Hence, different sequences of spontaneous emission will have different effects on a particular power dropout, e.g. the order in which the lasers drop and the later decision on the leader–laggard role. In order to study this effect, we perform Monte Carlo simulations of the rate equation model. By considering $\{\Delta\eta(t)\}$ as a stochastic variable, we are able to discern the effect of noise on the change of role. Each noise realization resembles the trace shown in figure 9(b), but the direction of the phase jumps changes with the realization. Figure 11(a) shows the mean value $\langle\Delta\eta(t)\rangle$ (solid curves) and the variance $\sigma^2(t) \equiv \langle\Delta\eta^2(t)\rangle - \langle\Delta\eta(t)\rangle^2$ (bold curves) of the relative injection phase. Now $\langle\cdot\rangle$ means average over 100 noise realizations. The phase difference displays an approximately zero mean, $\langle\Delta\eta(t)\rangle \approx 0$, when averaging over the different realizations. Hence, we deduce that $\Delta\eta(t)$ takes positive and negative values with the same probability. Moreover, we can observe a linear increase of the variance of $\{\Delta\eta(t)\}$ in time, $\sigma^2(t) \sim t$. From these results we conclude that the large jumps of the phase difference, associated with power dropouts of the achronal solution, can be regarded as a random walk driven by fluctuations [27].

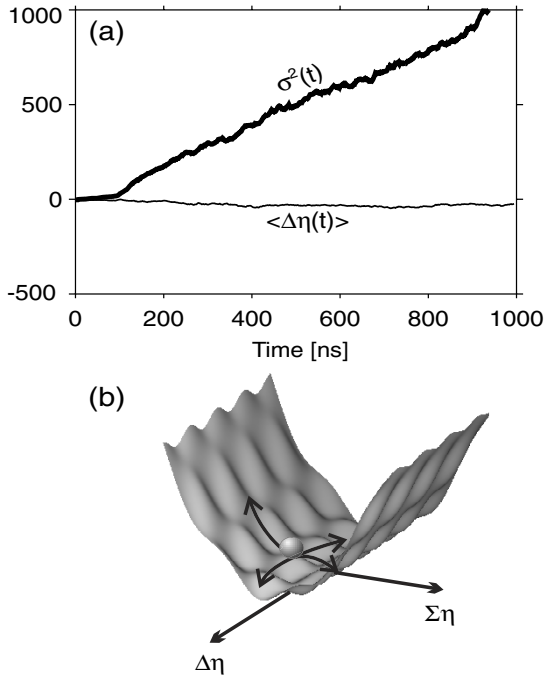

Figure 11. (a) Statistical properties of the injection phases under symmetric operation of the lasers, $I_1 = I_2 = I_{\mathrm{th}}^{\mathrm{sol}}$. (b) Movement of a Brownian particle in the thermodynamic potential given in equation (10).

6. Physical mechanisms

The interesting findings in section 5 motivate us to further investigate the mechanisms that cause the asymmetric roles of the two subsystems. In particular, it has been mentioned already that the governing equations are symmetric under the interchange of the lasers owing to the symmetric operating conditions. Thus, one might wonder why the solution where both lasers evolve at the same time (the isochronal solution) does not appear? The main observations can be summarized in the following points:

(i) The system spontaneously selects a state of achronal synchronization.
(ii) The isochronal solution is unstable for any small perturbation.
(iii) A change in the leader–laggard roles of the lasers may occur, in particular during power dropouts.

We are interested in finding a minimal description that simultaneously explains the above-mentioned features and, more importantly, that allow us to gain an insight into the underlying dynamics. We tackle the problem by introducing the idea of a thermodynamic potential. For the sake of simplicity, we neglect amplitude fluctuations in equations (4) and (5) to arrive at

$$d_t\,\varphi_{1,2}(t) = \kappa_c\sqrt{1+\alpha^2}\,\sin(\eta_{1,2}(t) + \varphi_0 + \arctan\alpha) + F_{\varphi_{1,2}}(t), \tag{7}$$

which describes the dynamical evolution of the phases associated with each oscillator as in Kuramoto's model with time delay [28]. Next, we assume small and slow variations of

the phases over a time τ, justifying the approximation [29]:

$$d_t\,\varphi_{1,2}(t) \approx -\frac{\eta_1(t)+\eta_2(t)}{2\tau} - \frac{1}{2} d_t\,\eta_{1,2}(t). \tag{8}$$

The resulting equations can be written more conveniently in the potential form

$$\frac{\mathrm{d}}{\mathrm{d}t}\eta_{1,2}(t) = -\frac{1}{\tau}\frac{\mathrm{d}}{\mathrm{d}\eta_{1,2}}U(\eta_1,\eta_2) + F_{\eta_{1,2}}(t), \tag{9}$$

$$U(\eta_1,\eta_2) = \tfrac{1}{2}(\eta_1+\eta_2)^2 - 2C[\cos(\eta_1+\varphi_0+\arctan\alpha) + \cos(\eta_2+\varphi_0+\arctan\alpha)], \tag{10}$$

with $C = \kappa_c\tau\sqrt{1+\alpha^2}$. For convenience, we express the potential in sum and difference variables, i.e. $\Sigma\eta = \eta_1+\eta_2$ and $\Delta\eta = \eta_1-\eta_2$. A typical shape of the thermodynamic potential $U(\Sigma\eta, \Delta\eta)$ is shown in figure 11(b). In spite of the simplicity of equation (9), it can provide an insightful interpretation of the underlying mechanisms. It is worth recalling that the extrema of the potential correspond to the monochromatic solutions. Let us consider a Brownian particle moving under the action of this potential. The movement is confined in the direction $\Sigma\eta$ because of the parabolic shape of the potential. The movement in such a direction is associated with the gradual decrease of both injection phases during consecutive power dropouts, as observed in figure 8(b). However, the potential is horizontal in the orthogonal direction, $\Delta\eta$, indicating that the particle can arbitrarily jump back and forth towards positive and negative values of $\Delta\eta$ due to fluctuations. Large amplitude fluctuations occur at the point of the power dropouts. Hence, the observed jumps in phase difference $\Delta\eta(t)$, in figure 9(b), stem from large excursions in the valley of the potential. Moreover, since the potential is horizontal in that direction, the particle undergoes a random-walk-like movement and the kicks on the particle can shift $\Delta\eta$ to higher or lower values with the same probability. This fact agrees with the results obtained from Monte Carlo simulations of the variable $\Delta\eta$ explained in section 5.4. Finally, the absence of any force pushing the particle towards the $\Delta\eta = 0$ manifold intuitively explains the instability of the isochronal solution that would require the manifold to be stable against fluctuations.

7. Concluding remarks

In conclusion, we have presented a detailed numerical and experimental investigation of the synchronization scenario that arises from the mutual optical coupling of two semiconductor lasers. We have found a two-threshold behaviour that appears upon variation of the symmetric mutual coupling strength. We obtained a first threshold, associated with the onset of coupling-induced instabilities, and a second threshold indicating the transition to synchronization. Despite the high degree of symmetry in the system, the solution spontaneously selected corresponds to an achronal state, i.e. a time shift between the dynamics of the two laser intensities is present. We have characterized the achronal solution using crosscorrelation analysis. We have found synchronization with a time shift of the subnanosecond pulsation of the laser intensities. This time shift corresponds to the coupling delay between lasers. The generalized return plots present a linear tendency only when a signal is time shifted. The attainable degree of synchronization is about 0.8–0.9. Although the achronal solutions distinguish between the lasers, statistical quantities (probability distribution, crosscorrelation etc) computed over long time intervals are invariant under the interchange of the lasers. The above-mentioned results are quite generic features that appear in a wide range of coupling strengths and injection currents covering the low frequency fluctuation and coherence collapse regimes.

It is worth remarking that the operation conditions occur within the (bidirectional) injection locking regime, as demonstrated by the existence of phase-locked monochromatic solutions [14]. However, our results indicate that the phase-locked operation associated with the isochronal solution becomes unstable, leading to a generalized (achronal) synchronization. This paper provides an intuitive explanation in terms of a thermodynamic potential. In this framework, this phase instability can be explained as the absence of any deterministic force pushing the system towards the synchronous state. Under symmetric operation, the presence of fluctuations induces a drift of the injection phases towards the direction of each of the lasers with same probability. The case of asymmetric operation treated in [10] is an interesting issue that deserves further investigation. Asymmetries can make the coupling more effective in one direction. Then, the driven system is pulled towards the driver. We have found that a preferential injection in one laser ($>1\%$ current difference), allows us to define a persisting leader that corresponds to the laser with larger injection. Then, a net drift on the difference in injection phases appears towards the direction of the laser with larger pumping. A similar behaviour can be also generated by slightly detuning ($\gtrsim$1 GHz) the emission frequency of the free-running lasers.

Acknowledgments

This work has been funded through the European Commission under Project OCCULT IST-2000-29683. JM and CRM also acknowledge funding from the Spanish MCyT under Project BFM2000-1108 and the MCyT and Feder BFM2001-0341-C01 and BFM2002-04369.

References

[1] Coffman K, McCormick W D and Swinney H L 1986 *Phys. Rev. Lett.* **56** 999
[2] Schäfer C, Rosenblum M G, Kurths J and Abel H H 1998 *Nature* **392** 239
[3] Ernst U, Pawelzik K and Geisel T 1995 *Phys. Rev. Lett.* **74** 1570
[4] Roy R and Thornburg K S Jr 1994 *Phys. Rev. Lett.* **72** 2009
[5] Mirasso C R, Colet P and García-Fernández P 1996 *IEEE Photon. Technol. Lett.* **8** 299
[6] Fischer I, Liu Y and Davis P 2000 *Phys. Rev.* A **62** 011801
[7] VanWiggeren G D and Roy R 1998 *Science* **279** 1198
[8] Jagher P C D, van der Graaf W A and Lenstra D 1996 *Quantum Semiclass. Opt.* **8** 805
[9] van Tartwijk G H M and Lenstra D 1995 *Quantum Semiclass. Opt.* **7** 87
[10] Hohl A, Gavrielides A, Erneux T and Kovanis V 1997 *Phys. Rev. Lett.* **78** 4745
[11] Hohl A, Gavrielides A, Erneux T and Kovanis V 1999 *Phys. Rev.* A **59** 3941
[12] Heil T *et al* 2001 *Phys. Rev. Lett.* **86** 795

[13] Fujino H and Ohtsubo J 2001 *Opt. Rev.* **8** 351
[14] Mulet J, Masoller C and Mirasso C R 2002 *Phys. Rev.* A **65** 063815
[15] Mirasso C R *et al* 2002 *Phys. Rev.* A **65** 013805
[16] Javaloyes J, Mandel P and Pieroux D 2003 *Phys. Rev.* A **67** 036201
[17] White J K, Matus M and Moloney J V 2002 *Phys. Rev.* E **65** 036229
[18] Agrawal G P and Dutta N K 1993 *Semiconductor Lasers* (New York: Van Nostrand-Reinhold)
[19] Fabiny L, Colet P, Roy R and Lenstra D 1993 *Phys. Rev.* A **47** 4287
[20] Pikovsky A S, Rosenblum M and Kurths J 2001 *Synchronization: a Universal Concept in Nonlinear Sciences* (New York: Cambridge University Press)
[21] Rosenblum M G, Pikovsky A S and Kurths J 1996 *Phys. Rev. Lett.* **76** 1804
[22] Rosenblum M G, Pikovsky A S and Kurths J 1997 *Phys. Rev. Lett.* **78** 4193
[23] Tkach R W and Chraplyvy A R 1986 *IEEE J. Lightwave Technol.* **4** 1655
[24] Lenstra D, Verbeek B H and den Boef A J 1985 *IEEE J. Quantum Electron.* **21** 674
[25] van Tartwijk G H M, Levine A M and Lenstra D 1995 *IEEE J. Sel. Top. Quantum Electron.* **1** 446
[26] Mulet J and Mirasso C R 1999 *Phys. Rev.* E **59** 5400
[27] San Miguel M and Toral R 2000 Stochastic effects in physical systems *Proc. Instabilities and Non-Equilibrium Structures* vol 6, ed J M E Tirapegui and W Tiemann (Dordrecht: Kluwer–Academic) p 35
[28] Yeung M K S and Strogatz S H 1999 *Phys. Rev. Lett.* **82** 648
[29] Mørk J, Semkow M and Tromborg B 1990 *Electron. Lett.* **26** 609